Journal of Nanobiotechnology

RESEARCH

Open Access

Au-modified ceria nanozyme prevents and treats hypoxia-induced pulmonary hypertension with greatly improved enzymatic activity and safety

Rui Xiao[1,2†], Jia Liu[3†], Lin Shi[3,4†], Ting Zhang[1,2], Jie Liu[1,2], Shuyi Qiu[1,2], Matthieu Ruiz[5,6], Jocelyn Dupuis[6,7], Liping Zhu[1,2*], Lin Wang[3,4*], Zheng Wang[3,8*] and Qinghua Hu[1,2*]

Abstract

Background Despite recent advances the prognosis of pulmonary hypertension remains poor and warrants novel therapeutic options. Extensive studies, including ours, have revealed that hypoxia-induced pulmonary hypertension is associated with high oxidative stress. Cerium oxide nanozyme or nanoparticles (CeNPs) have displayed catalytic activity mimicking both catalase and superoxide dismutase functions and have been widely used as an anti-oxidative stress approach. However, whether CeNPs can attenuate hypoxia-induced pulmonary vascular oxidative stress and pulmonary hypertension is unknown.

Results In this study, we designed a new ceria nanozyme or nanoparticle (AuCeNPs) exhibiting enhanced enzyme activity. The AuCeNPs significantly blunted the increase of reactive oxygen species and intracellular calcium concentration while limiting proliferation of pulmonary artery smooth muscle cells and pulmonary vasoconstriction in a model of hypoxia-induced pulmonary hypertension. In addition, the inhalation of nebulized AuCeNPs, but not CeNPs, not only prevented but also blunted hypoxia-induced pulmonary hypertension in rats. The benefits of AuCeNPs were associated with limited increase of intracellular calcium concentration as well as enhancement of extracellular calcium-sensing receptor (CaSR) activity and expression in rat pulmonary artery smooth muscle cells. Nebulised AuCeNPs showed a favorable safety profile, systemic arterial pressure, liver and kidney function, plasma Ca^{2+} level, and blood biochemical parameters were not affected.

†Rui Xiao, Jia Liu and Lin Shi contributed equally to this work.

*Correspondence:
Liping Zhu
16654396@qq.com
Lin Wang
lin_wang@hust.edu.cn
Zheng Wang
zhengwang@hust.edu.cn
Qinghua Hu
qinghuaa@mails.tjmu.edu.cn

Full list of author information is available at the end of the article

Conclusion We conclude that AuCeNPs is an improved reactive oxygen species scavenger that effectively prevents and treats hypoxia-induced pulmonary hypertension.

Graphical Abstract

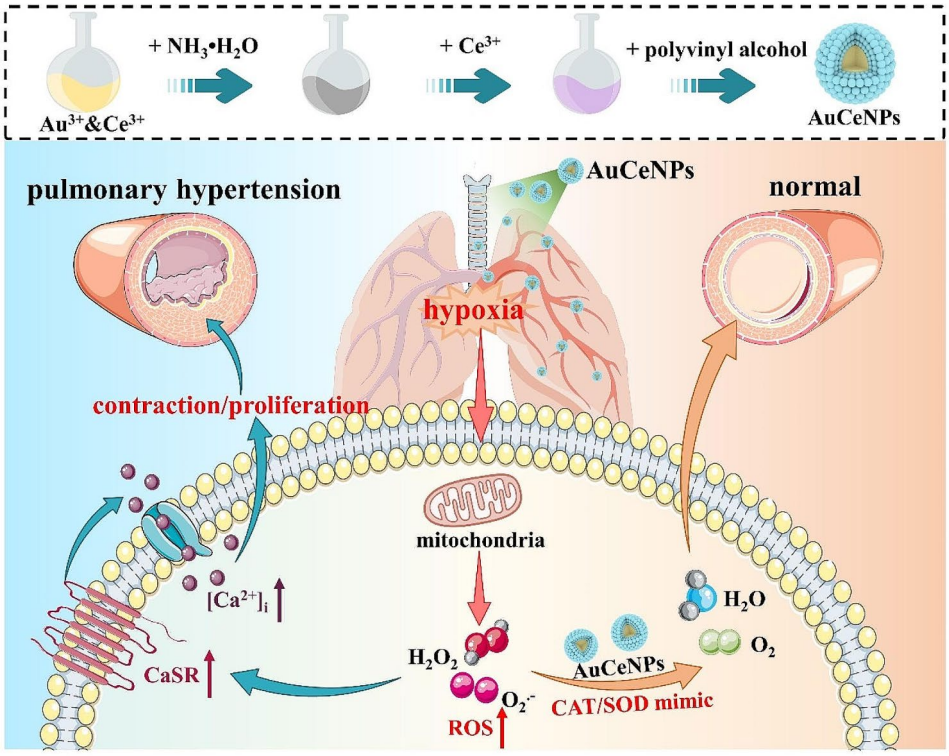

Keywords Pulmonary hypertension, Hypoxia, CaSR, Cerium oxide, Au

Background

Pulmonary hypertension (PH) is characterized by pulmonary vasoconstriction and remodeling, resulting in increased pulmonary vascular resistance as well as right ventricular afterload, eventually leading to right heart failure and death [1–3]. There are three major classes of medications to treat the various groups of pulmonary arterial hypertension including prostacyclin analogues, endothelin receptor antagonists and nitric oxide regulators. These drugs have shown efficacy mostly in group 1 subjects suffering from pulmonary arterial hypertension (PAH). The latest guidelines state that there is limited and conflicting evidence for the use of medication approved for PAH in patients with group 3 PH [4], the medications for PAH medication is not recommended for patients with group 3 PH.

Despite many efforts to develop new therapeutic options, there is unfortunately a lack of specific and efficient therapeutic strategies for subjects with group 3 pulmonary hypertension which is associated with chronic lung disease and/or hypoxia.

Our previous studies have shown that hypoxic conditions enhance the activity and expression of the extracellular calcium-sensing receptor (CaSR) subsequent to the release of mitochondria-derived reactive oxygen species (ROS) in pulmonary artery smooth muscle cells (PASMCs). The CaSR activation leads to increased intracellular Ca^{2+} concentration ($[Ca^{2+}]_i$) and higher proliferation rate of PASMCs ultimately promoting vascular constriction and remodeling leading to pulmonary hypertension [5, 6]. Consistent with the role of ROS in the development of hypoxic pulmonary hypertension [5–9], it has been reported that overexpressing of superoxide dismutase (SOD), catalase (CAT) or using antioxidants can improve hypoxia-induced pulmonary hypertension [10–13]. Antioxidant-based therapeutic approaches could therefore be explored in the prevention and treatment of pulmonary hypertension.

Recently, nanomaterials with enzymatic catalytic activities, named nanozymes, have been developed. Nanozymes offer the advantages being less expensive, having higher enzyme stability and programmable enzymatic ability [14, 15]. Many nanozymes acting as ROS

scavengers have been shown to attenuate ROS-induced cell toxicity and damages to a similar manner than natural antioxidant enzymes [16, 17]. Among them, ceria nanoparticles (CeNPs) are versatile and biocompatible nanozymes and were reported at the beginning of the 21st century to be an antioxidant for scavenging free radicals because of the presence of the mixed valence states of Ce^{3+} and Ce^{4+} on the surface [18, 19]. In 2007, it was first reported to be applied in vivo, reducing myocardial oxidative stress, and improving cardiomyopathy through its own regenerative antioxidant properties [20]. CeNPs have a catalytic activity mimicking both catalase (CAT) and superoxide dismutase (SOD) antioxidant capacities according to the following mechanisms [21]:

$$Ce^{3+} + O_2^{-} + 2H^{+} \rightarrow Ce^{4+} + H_2O_2;$$
$$Ce^{4+} + H_2O_2 \rightarrow Ce^{3+} + 2H + +O_2.$$

These characteristics enable CeNPs to be widely examined in different fields of biomedicine research, for example, protecting rodent lungs from hypobaric hypoxia-induced oxidative stress and inflammation [22], attenuating ischemia-reperfusion injury [23–25], alleviating tumor hypoxia [26, 27], and beneficial for neurodegenerative diseases [28, 29]. In addition, Amin et al. reported that CeNPs protected the liver from oxidative damage induced by monocrotaline (MCT) [30]. Kolli et al. reported that CeNPs (i.v. injection at a dose of 0.1 mg/kg) attenuated MCT-induced right ventricular hypertrophy [31] and Nassar et al. reported that CeNPs (twice per week by i.p. injection at a dose of 0.5 mg/kg) attenuated MCT-induced pulmonary hypertension and associated right ventricular hypertrophy [32]. While these previous findings are related to models of group 1 pulmonary hypertension, whether CeNPs can attenuate hypoxia-induced pulmonary hypertension, belonging to group 3 pulmonary hypertension, is still unknown.

The catalytic activities of CeNPs depend on the redox-oxidation cycle between Ce^{3+} and Ce^{4+}, however the reduction process from Ce^{4+} to Ce^{3+} is energetically impeded, which limits the antioxidant capability of CeNPs [33, 34]. Thus, in this study, we introduced gold (Au) nanocore to ceria nanoparticles, being named $AuCeO_2$ nanoparticles (AuCeNPs), to enhance the electron transfer and accelerate the reduction rate of Ce^{4+} for strengthening the enzymatic catalytic activities [35]. We administered AuCeNPs to rats through nebulized inhalation to increase their lung bioavailability, and we comprehensively evaluated the effects of AuCeNPs on hypoxia-induced pulmonary hypertension in both preventive and therapeutic protocols.

Methods

Ethical approval

All procedures performed in animals were approved by the Institutional Animal Care and Use Committee of Tongji Medical College, Huazhong University of Science and Technology, and according to the guidance of the National Institutes of Health. Hemodynamics was monitored in rats after anesthesia by intraperitoneal injection of pentobarbital sodium at a dose of 30 mg/kg [36, 37]. Euthanasia was performed using pentobarbital injection (180 mg/kg, IP).

Materials

Chloroauric acid ($HAuCl_4.4H_2O$), riboflavine, L-methionine, nitrotetrazolium blue chloride (NBT) and were purchased from Aladdin Industrial Corporation (Shanghai, China). Cerium nitrate hexahydrate [$Ce(NO_3)_3.6H_2O$], ammonia solution (25%~28%) and hydrogen peroxide (H_2O_2, 30%) were provided by Sinopharm Chemical Regent Co., Ltd (Shanghai, China). 2,7-Dichlorofluorescin diacetate (DCFH-DA) were purchased from Sigma-Aldrich (USA). Methylthiazolyldiphenyl-tetrazolium bromide (MTT) was purchased from Solarbio company. Hydrogen peroxide assay kit (Cat No. S0038), calcein acetoxymethyl ester (Calcein-AM), propidium iodide (PI) were obtained from Beyotime biotechnology company (China). Ultrapure water (18.2 MΩ/cm at 25 °C) purified by a Milli-Q system was used throughout the experiment.

Synthesis of AuCeNPs

AuCeNP was synthesized by a simple hydrothermal redox reaction as previously reported with little modification [38]. Briefly, the $HAuCl_4$ solution (0.024 M, 600 μL) and $Ce(NO_3)_3$ solution (0.1 M, 1.4 mL) were dissolved in pre-cooled deionized water (50 mL), and freshly prepared ammonia solution (0.313 M, 3 mL) was added into the mixture solution. Then additional $Ce(NO_3)_3$ solution (0.0467 M, 3 mL) was immediately added and kept stirring for 15 min. After that, the mixture was added into 10 mL polyvinyl alcohol (1% w/v) and stirred in ice bath for another 1 h. Finally, the pellet obtained after centrifugation (10,000 g for 40 min at 10 °C) was washed three times with deionized water and store at 4 °C for later use.

Characterizations

The morphology of AuCeNPs were observed by transmission electron microscopy (JEM-2100 F, Japan). Energy-dispersive X-ray spectroscopy was performed with a Xflash 5030 detector (Brucker, Germany). X ray photoelectron spectroscopy (XPS) was performed on a Thermo Fisher Scientific K-Alpha using a monochromatic Al Kα X ray source. Dynamic light scattering (DLS) measurements were carried out using Zetasizer

Nano series (Malvern 2000, USA). Elemental analysis for sample determination was performed by an inductively coupled plasma atomic emission spectrometer (ICP-AES; iCAP 7000 Series ICP Spectrometer). The OD value of samples was detected by a multifunctional microplate reader (Victor Nivo™, USA).

CAT activity assay of AuCeNPs

Hydrogen peroxide assay kit (Cat No. S0038, Beyotime) was used to evaluate the catalase activity of AuCeNPs. Briefly, hydrogen peroxide solution (10 mmol/L) was incubated for 2 h with different concentrations of AuCeNPs (0–200 μg/mL). Then, the AuCeNPs were removed by centrifugation and the concentration of H_2O_2 remaining in the supernatant was detected using the hydrogen peroxide assay kit. The inhibition rate of H_2O_2 was calculated as follows: inhibition (%) = $[(A_0 - A)/A_0] \times 100\%$, where A_0 is the absorbance of the solution without AuCeNPs and A is the absorbance of the solution with different concentration of AuCeNPs.

SOD activity assay of AuCeNPs

The SOD-like activity of AuCeNPs (scavenging superoxide anion) was evaluated using the total superoxide dismutase activity assay kit (Elabscience) according to the manufacturers' instruction.

In vitro biocompatibility evaluation of AuCeNPs

HUVEC (1–0025, CHI Biotechnology Co., Ltd, Jiangsu, CHINA) and PASMC were seeded in 96-well culture plates (8,000 cells per well) and incubated for 24 h. Then, the media were replaced with fresh media containing AuCeNPs (0–200 μg/mL). After 24 h incubation, the viability of cells in 96-well plates was tested using MTT assay. The hemolysis assay was performed with previously reported methods [39].

ROS detection

The detection of ROS in pulmonary artery smooth muscle cells was performed using the Reactive Oxygen Species Assay Kit (S0033S, Beyotime) according to the manufacturer's instructions. Briefly, after removing the cell culture medium, 10 μmol/L DCFH-DA was added to the cells and incubated for 20 min. Cells were washed three times with serum-free medium and observed directly with a laser confocal microscope using an excitation wavelength of 488 nm and an emission wavelength of 525 nm. Each measure was repeated 5 times, and the fluorescence intensity of each group was counted.

H_2O_2 content detection

The detection of H_2O_2 content in pulmonary artery smooth muscle cells was performed using the Hydrogen Peroxide Assay Kit (S0038, Beyotime) according to the manufacturer's instructions. Pulmonary artery smooth muscle cells were digested from the culture dish with trypsin and collected into EP tubes, and a part of the cell suspension was taken for cell counting. The remaining cell suspension was centrifuged at 1,000 g at 4 °C for 10 min, the supernatant was discarded, and the cell pellet was kept. Lysis buffer (100 μL/10^6 cells) was added to the cell pellet, followed by extensive homogenization to promote the lysis of the cells. The lysate was then centrifuged at 12,000 g for 5 min at 4 °C, and the supernatant kept for subsequent analysis. Fifty μL of sample or H_2O_2, as positive standard, was added to the well and completed with 100 μL of H_2O_2 detection reagent. After gentle shaking, the absorbance was measured at a wavelength of 560 nm after a 30-minuite incubation at room temperature. The concentration of H_2O_2 in the sample was calculated according to the standard curve established by an incremental series of H_2O_2 concentration at 1, 3, 10, 30, 100 μmol/L.

Uptake and metabolism of AuCeNPs in vivo

The Sprague Dawley rats were treated with AuCeNPs at a dose of 0.5 mg/kg by nebulized inhalation and pulmonary arteries of rats were immediately dissected after nebulized inhalation for transmission electron microscopy to observe whether AuCeNPs can be delivered to PASMCs. In addition, the pulmonary arteries of rats were also dissected at different time points after nebulized inhalation (0, 4, 8, 24, 48, 72, 168 h), digested with aqua regia, and the gold content was detected by inductively coupled plasma atomic emission spectrometry (ICP-AES). The metabolism of AuCeNPs was estimated by the content of Au element.

Animal model and treatment

Pulmonary hypertension was induced in rats by chronic hypoxia as we previously reported [40]. Briefly, SD rats (approximately 200 g) were exposed to 10% O_2 for 4 weeks in a chamber. The oxygen content in the chamber was balanced with N_2. CeNPs or AuCeNPs was delivered by nebulized inhalation as described in our previous report [6] at 0.5 mg/kg [32]. In the preventive model, during the four-week period of chronic exposure to hypoxia, CeNPs and AuCeNPs were delivered by nebulized inhalation every other day at a dose of 0.5 mg/kg for a total of 14 times. In the therapeutic model, during the 5th and 6th weeks of chronic exposure to hypoxia, CeNPs and AuCeNPs were delivered by nebulized inhalation every other day at a dose of 0.5 mg/kg for a total of 7 times.

Nebulized inhalation

When preparing for nebulized inhalation, rats were taken out of a glass chamber for hypoxia (86×66×36 cm^3) and placed in another glass chamber for nebulized inhalation

($40\times40\times26$ cm^3). The CeNPs or AuCeNPs were prepared at the dose of 0.5 mg/kg body weight, dissolved in 5 mL sterile saline and pooled into the nebulizer (NE-C25S, OMRON), which was connected to the glass chamber for nebulized inhalation. The chamber housed 5 rates (~280 g/rat) for each atomization, which last for about 15 min. During the nebulized inhalation, the padding was replaced, and the food and water were replenished in the glass chamber for hypoxia.

Detailed descriptions regarding to the following methods have been previously described and are now supplied in the supplement: PASMCs culture [5, 40], $[Ca^{2+}]_i$ measurement [5, 40], measurement of isometric tension of PA rings [5, 40], western blot [41], plasma Ca^{2+}, blood routine analysis, liver and renal function, RV and pulmonary morphometry analysis.

Statistical analysis

The experimental results were expressed as mean ± SE. Normally distributed data was analyzed by Student t tests (two groups) and one-way ANOVA (more than two groups) followed by Student-Newman-Keuls post hoc multiple groups comparisons. Non-normally distributed data was analyzed by Mann-Whitney rank sum or Kruskal Wallis tests followed by Dunn's multiple groups comparisons. A statistical difference was set at $P<0.05$.

Results

Synthesis and characterizations of AuCeNPs

The $AuCeO_2$ was synthesized by one-step redox reaction between Ce^{3+} and $AuCl_4^-$ that produced a purple homogeneous suspension in aqueous solution. Transmission electron microscopy (TEM) showed a uniform distribution of $AuCeO_2$ (Fig. 1A). High-resolution transition electron microscopy (HRTEM) imaging illustrated the distinct lattice fringes of ceria nanoparticles (0.314 nm) and gold nanoparticles (0.28 nm). The ceria nanoparticles were stacked around the Au core (7.40 nm), forming a typical core-shell structure (25.50 nm) (Fig. 1A and C). High-angle annular dark-field (HAADF)-STEM

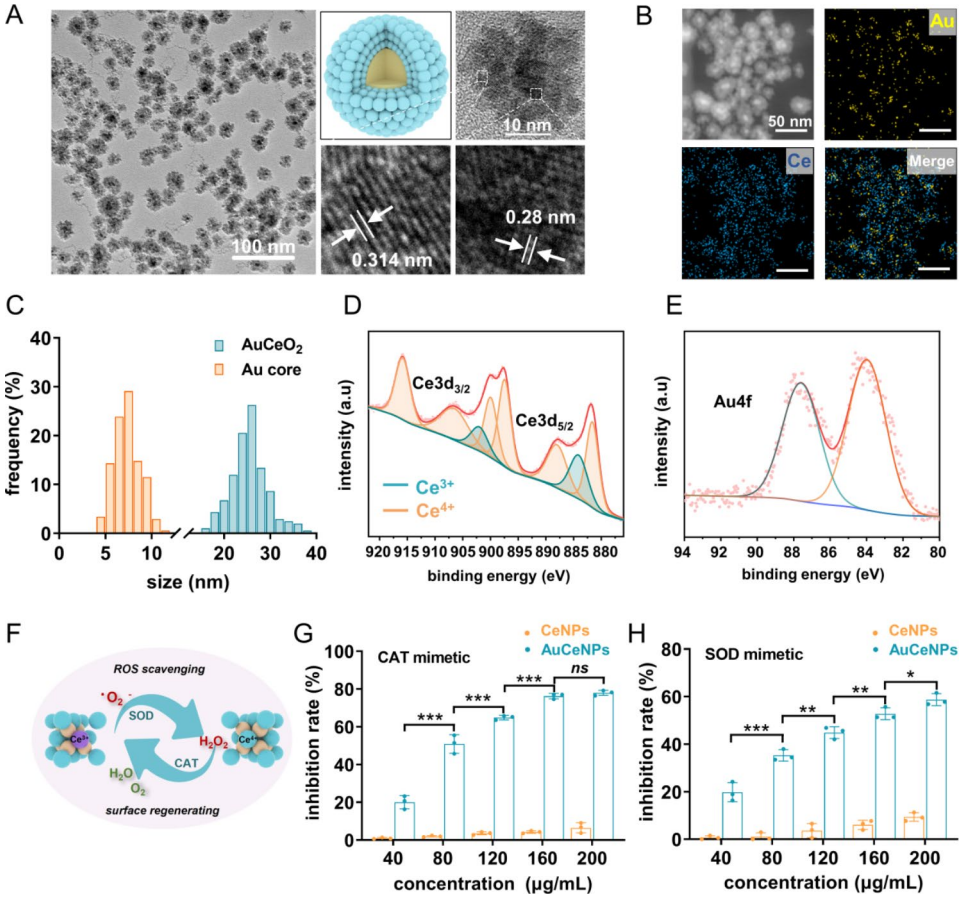

Fig. 1 Characterizations of AuCeNPs. TEM (left) and HRTEM (right) images of $AuCeO_2$ (**A**). STEM-EDS elemental mapping images of $AuCeO_2$ (scale bar, 50 nm, **B**). $AuCeO_2$ and Au core size distribution histogram (**C**). XPS of ceria NPs and Au NPs. Ce^{3+} peaks at 884.1 and 902.0 eV, Ce^{4+}peaks at 881.6, 887.9, 897.4, 900.0, 906.5 and 915.8 eV (**D–E**). Schematic illustrations of CAT and SOD mimicing activity of AuCeNPs (**F**). H_2O_2 scavenging ability of AuCeNPs and commercialized Ceria NPs at different concentrations (**G**, *** $p<0.001$, $n=3$). $O_2^{\bullet-}$ scavenging ability of AuCeNPs and commercialized Ceria NPs at different concentrations (**H**, *** $p<0.001$, ** $p<0.01$. * $p<0.05$, $n=3$). One-way ANOVA followed by Student-Newman-Keuls for multiple groups comparisons

combined with energy-dispersive spectroscopy (EDS) further revealed the spatial distribution of Ce and Au in the $AuCeO_2$ (Fig. 1B), confirming the core-shell structure of $AuCeO_2$. The Au content in the $AuCeO_2$ was determined to be 9.43 wt% by inductively coupled plasma-atomic emission spectrometry (ICP-AES). X-ray photoelectron spectroscopy (XPS) spectra exhibited the characteristic peaks of Ce and Au on 3d and 4f orbitals, respectively (Fig. 1D-E). Specifically, Ce^{3+} (peaks at 884.1 and 902.0 eV) and Ce^{4+} (peaks at 881.6, 887.9, 897.4, 900.0, 906.5 and 915.8 eV) ions coexisted in the $AuCeO_2$, where the ratio of Ce^{3+}/Ce^{4+} was 0.22 (Fig. 1D). Due to the low redox potential of Ce^{3+}/Ce^{4+}, the Ce ions can be easily switched in the process of interaction with reactive oxygen species [35], which ensures the regenerative antioxidant activity of $AuCeO_2$ (Fig. 1F). To increase the colloidal stability, the $AuCeO_2$ were encapsulated with polyvinyl alcohol (PVA, a negatively-charged and hydrophilic polymer) and the hydrodynamic diameter and ζ-potential of the PVA-coated nanoparticles (termed AuCeNPs) were 47.41 nm and 8.54 mV, respectively (Fig. S1).

Next, the antioxidant activity of AuCeNPs were studied by scavenging hydrogen peroxide (H_2O_2) and superoxide anion ($O_2^{\bullet-}$), mimicking CAT and SOD activities respectively. The commercial ceria nanoparticles (CeNPs, 89.0 nm, Aladdin Industrial Corporation) were set as the control (Figure S2). We observed that AuCeNPs greatly scavenged the H_2O_2 and $O_2^{\bullet-}$ in a dose dependent manner (Fig. 1G-H). At the serials concentrations from 40 to 200 μg/mL, the inhibition rates of H_2O_2 and $O_2^{\bullet-}$ were far higher than those of commercialized ceria nanoparticles (CeNPs) at the same concentrations (Fig. 1G-H). These results demonstrate that the AuCeNPs possess higher CAT- and SOD-mimicking activities than the commercial CeNPs, likely because that AuCeNPs contain higher contents of Ce^{3+} and possess enhanced electron transfer capability induced by Au nanocore compared with CeNPs (Figure S2) [35].

AuCeNPs inhibits hypoxia-induced increase of ROS in pulmonary artery smooth muscle cells

The biocompatibility of AuCeNPs was investigated in vitro. After exposure to AuCeNPs (25–400 μg/mL) for 24 h, the viability of both human umbilical vein endothelial cells (HUVECs) and pulmonary artery smooth muscle cells (PASMCs) was unchanged in comparison with the untreated group (Fig. 2A). Moreover, the hemolysis activity of AuCeNPs was less than 5%, even at the higher tested concentration of 500 μg/mL (Fig. 2B). These results demonstrate the good biocompatibility of AuCeNPs in vitro.

Whether AuCeNPs can scavenge reactive oxygen species (ROS) by mimicking the CAT and SOD in PASMCs was then explored. Twenty-four hours of hypoxia induced a significant increase in ROS content in PASMCs and AuCeNPs (10 μg/mL) significantly inhibited the hypoxia-induced increase of ROS content in PASMCs (Fig. 2C-D) while unmodified CeNPs did not decrease ROS levels. AuCeNPs did not show any effect on the ROS content in PASMCs under normoxia (Fig. 2C-D). A similar phenomenon was also observed for H_2O_2 concentration in PASMCs: 24 h of hypoxia induced a significant increase of H_2O_2 content in PASMCs compared with the normoxia group (1.73±0.09 mmol/g protein, $n=9$, $p<0.001$ versus 0.64±0.04 mmol/g protein for normoxia; Fig. 2E). AuCeNPs significantly reduced hypoxia-induced increase of H_2O_2 in PASMC, to a greater extent than with unmodified CeNPs, as compared with the hypoxic condition without AuCeNPs (0.77±0.05 mmol/g protein, $n=9$, $p<0.001$ versus 1.73±0.09 mmol/g protein for hypoxia; Fig. 2E). Similarly, AuCeNPs had no significant effect on the concentration of H_2O_2 in PASMCs under normoxia (0.59±0.03 mmol/g protein, $n=9$, Fig. 2E).

AuCeNPs blunts hypoxia-induced increase of intracellular calcium concentration and proliferation of pulmonary artery smooth muscle cells

In order to explore the effect of AuCeNPs on the intracellular calcium concentration ($[Ca^{2+}]_i$) in PASMCs cultured under normoxia or hypoxia, we used the fluorescence intensity ratio of fura 2-AM under excitation light of 340 nm and 380 nm to reflect the $[Ca^{2+}]_i$ as we previously reported [5, 6, 40, 42, 43]. We found that the $[Ca^{2+}]_i$ in PASMCs exposed to 1% O_2 for 48 h was significantly increased (fura 2-ratio=4.54±0.20, $n=15$ cells from 5 independent experiments, $p<0.001$ versus 2.83±0.19 for normoxia, Fig. 3A-C). AuCeNPs, in contrast to CeNPs, significantly inhibited the increase of $[Ca^{2+}]_i$ induced by hypoxia in PASMCs (3.62±0.17, $n=14$ cells from 5 independent experiments, $p<0.05$ versus 4.54±0.20 for hypoxia, Fig. 3C). AuCeNPs had no effect on the $[Ca^{2+}]_i$ in PASMCs under normoxic state (Fig. 3C).

To explore whether AuCeNPs can inhibit hypoxia-induced PASMCs proliferation, a CCK-8 assay was employed. Exposure to 1% O_2 for 24 h stimulated a rapid growth of PASMCs (178.64±6.62%, $n=5$, $p<0.001$ versus 100.00±2.23% for normoxia, Fig. 3D). AuCeNPs, but not CeNPs, significantly inhibited this hypoxic proliferation response (124.88±6.26%, $n=5$, $p<0.001$ versus 178.64±6.62% for hypoxia; Fig. 3D). However, AuCeNPs had no effect on PASMCs growth under normoxia (Fig. 3D).

AuCeNPs attenuates hypoxic pulmonary vasoconstriction

In order to explore whether AuCeNPs influences hypoxic pulmonary vasoconstriction, we studied the tension of isolated vascular rings. In pulmonary artery (PA)

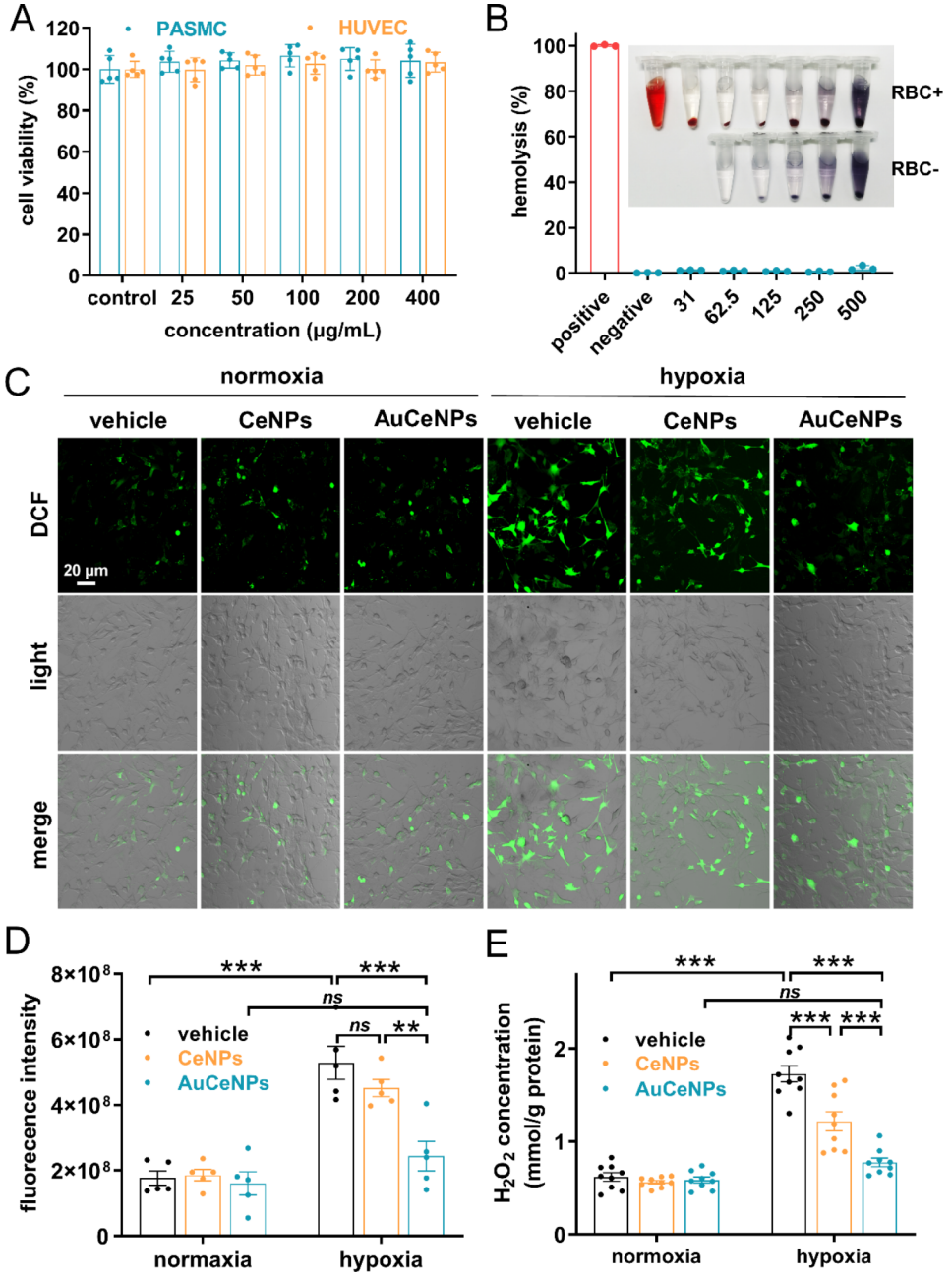

Fig. 2 AuCeNPs inhibits hypoxia-induced increase of ROS in pulmonary artery smooth muscle cells (PASMCs). Cell viability (%) of PASMCs and HUVECs (**A**) treated with AuCeNPs. Hemolysis activity of AuCeNPs (**B**). Representative images of DCFH-DA fluorescence in PASMCs (**C**). Histograms of DCFH-DA fluorescence intensity in PASMCs (**D**, ***$p < 0.001$, **$p < 0.01$, $n = 5$). Statistics of H_2O_2 concentration in PASMCs (**E**, ***$p < 0.001$, **$p < 0.01$, $n = 9$). One-way ANOVA followed by Student-Newman-Keuls for multiple groups comparisons

rings with removed endothelium, hypoxia significantly increased the tension even greater than 28% of the 80 mmol/L K^+ (KCl-physiological saline solution)-induced tension (28.32±1.22% and 28.39±0.96% for the first and second stimuli respectively; Fig. 4A and D). AuCeNPs (10 μg/mL) attenuated hypoxia-induced constriction to 12.13±0.65% (n=3, p<0.001, Fig. 4C and **D**), while CeNPs had no effect.

AuCeNPs prevents and reverses hypoxia-induced pulmonary hypertension in rats

Collectively, the above-mentioned results show that AuCeNPs inhibited hypoxia-induced ROS and $[Ca^{2+}]_i$ increase in PASMCs, PASMCs proliferation, and pulmonary vasoconstriction. Here, we further explored whether AuCeNPs can attenuate pulmonary hypertension induced by hypoxia "in vivo" in both preventive (Fig. 5) and therapeutic models (Fig. 6).

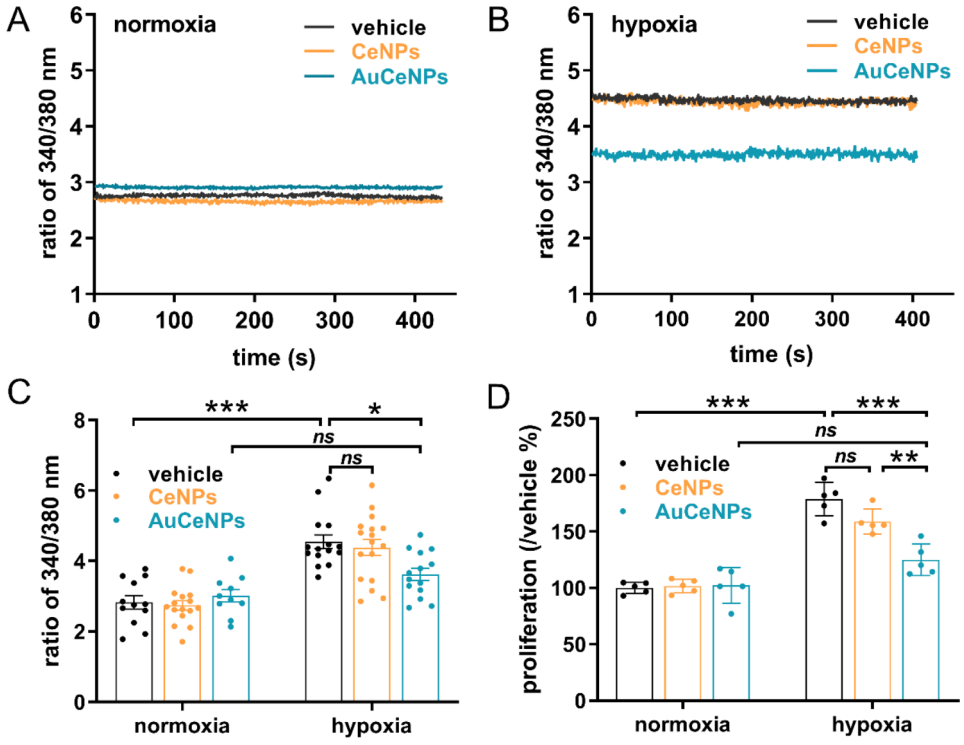

Fig. 3 AuCeNPs reverses hypoxia-induced increase in intracellular calcium concentration and proliferation of pulmonary artery smooth muscle cells (PASMCs). Representative traces of fura 2-AM fluorescence intensity ratio under 340 nm and 380 nm excitation light in pulmonary artery smooth muscle cells (PASMCs) under normoxia (**A**) and hypoxia (**B**). Histograms of fura 2-AM fluorescence intensity ratio under 340 nm and 380 nm excitation light in PASMCs (**C**, ***$p<0.001$, *$p<0.05$, $n=10$–17 cells from 5 independent experiments) and PASMCs proliferation (**D**, ***$p<0.001$, **$p<0.01$, $n=5$). One-way ANOVA followed by Student-Newman-Keuls for multiple groups comparisons

In order to improve selective targeting of lung tissue, AuCeNPs were administered to rats by nebulized inhalation at a dose of 0.5 mg/kg. To confirm whether AuCeNPs can be delivered to PASMCs through this approach, the pulmonary artery smooth muscle layer of rats was separated and used for gold immunoelectron microscopy at the end of nebulized inhalation. We found that the particles were clearly identified in PASMCs (Figure S3A), indicating that AuCeNPs were successfully locally delivered to PASMCs. We then examined the kinetic distribution of AuCeNPs in pulmonary arteries. After nebulized inhalation of AuCeNPs, the pulmonary arteries of rats were separated at different time points, digested with aqua regia and the content of Au was detected by inductively coupled plasma atomic emission spectrometry (ICP-AES). We found that the half-life of AuCeNPs was about 48 h (S3B). The frequency of AuCeNPs administration was thus determined to be once every other day.

Figure 5A shows our experimental procedure to address the impact of AuCeNPs administrated in a preventive mode by nebulized inhalation (every other day at a dose of 0.5 mg/kg) from the first day of hypoxia exposure. AuCeNPs significantly reduced parameters of pulmonary hypertension: (i) mean pulmonary artery pressure (mPAP, from 26.62±0.90 to 18.01±1.42 mmHg, $p<0.001$, Fig. 5B), (ii) pulmonary vascular resistance (PVR, from 279.60±25.94 to 177.01±21.03 mmHg·L/min, $p<0.01$, Fig. 5C), (iii) right ventricular hypertrophy (RV/(LV+S), from 0.38±0.01 to 0.32±0.01, $p<0.001$, Fig. 5D) and pulmonary vascular remodeling (thickness from 54.23±3.76% to 41.36±1.36%, $p<0.001$, Fig. 5F-G). In contrast, hypoxic rats receiving commercial CeNPs did not show any improvement and both CeNPs and AuCeNPs did not show any effect on mean systemic arterial pressure (mSAP, Fig. 5E). Hypoxia induced significant increases in MDA and 8-OHdG in pulmonary arteries of rats, and AuCeNPs, rather than CeNPs, significantly reduced the increase in MDA and 8-OHdG (Fig. 5H-I).

Figure 6A shows our experimental procedure to address the impact of AuCeNPs administrated in a therapeutic mode when nebulized by inhalation (every other day at a dose of 0.5 mg/kg) from the fifth week of hypoxia exposure. The administration of AuCeNPs significantly reduced parameters of pulmonary hypertension induced by hypoxia: (i) mean pulmonary artery pressure (mPAP, from 32.52±4.09 to 24.38±3.10 mmHg, $p<0.05$, Fig. 6B), (ii) pulmonary vascular resistance (PVR, from 344.43±40.89 to 206.69±23.49 mmHg·L/min, $p<0.01$, Fig. 6C), (iii) right ventricular hypertrophy (RV/(LV+S), from 0.61±0.03 to 0.40±0.03, $p<0.001$, Fig. 6D) and

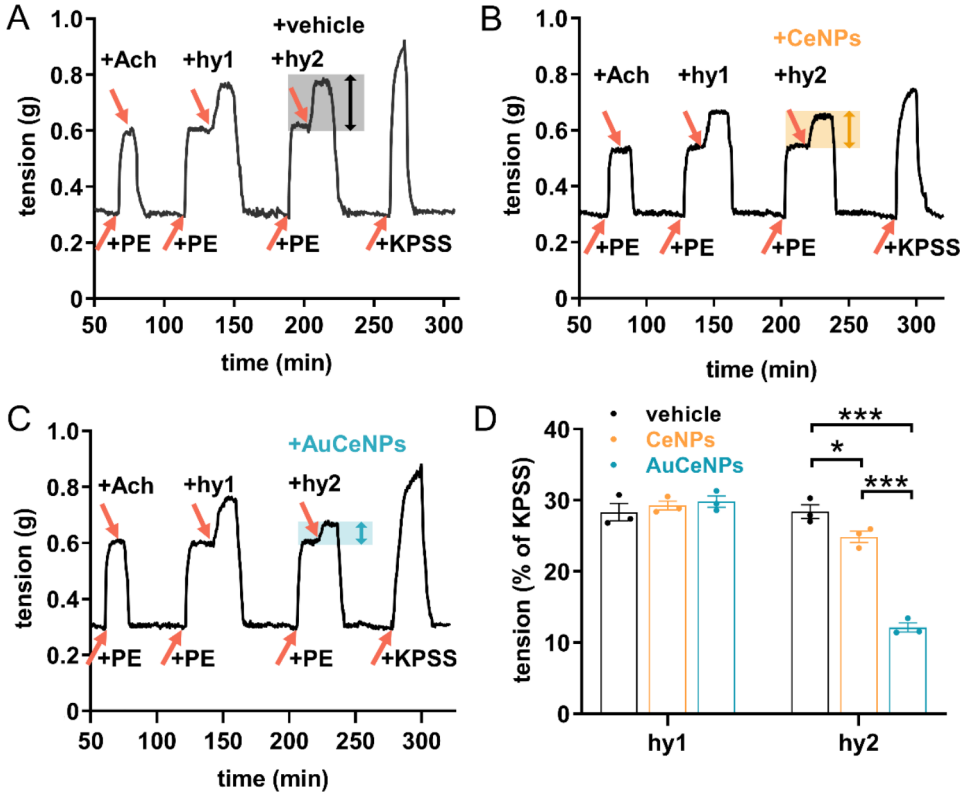

Fig. 4 AuCeNPs attenuates hypoxic pulmonary vasoconstriction. Isometric tension of endothelium removed pulmonary artery (PA) rings preconstricted by phenylephrine (PE) in response to acetylcholine (Ach) and two sequential episodes of hypoxia (hy1 and hy2) followed by a final exposure of 80 mM K^+ (KCl physiological salt solution (KPSS) in the presence of the vehicle (**A**), CeNPs at 10 μg/mL (**B**) or AuCeNPs at 10 μg/mL (**C**) added during the second episode of hypoxia (hy2), normalized to the tension induced by KPSS (***$p<0.001$, *$p<0.05$, $n=3$, **D**). One-way ANOVA followed by Student-Newman-Keuls for multiple groups comparisons

pulmonary vascular remodeling (thickness from 60.40±1.03% to 43.21±0.43%, $p<0.001$, Fig. 6F-G). In contrast, hypoxic rats receiving CeNPs without Au modification did not show any improvement except for right ventricular hypertrophy. Both CeNPs and AuCeNPs did not show any effect on mean systemic arterial pressure (mSAP, Fig. 6E). Hypoxia induced significant increases in MDA and 8-OHdG in pulmonary arteries of rats, and AuCeNPs, rather than CeNPs, significantly reduced the increase in MDA and 8-OHdG (Fig. 6H-I).

In addition, liver and kidney function, plasma Ca^{2+} level, and other blood biological parameters of rats in preventive and therapeutic protocols remained unaffected by the administration of AuCeNPs (Figs.S4-S7), indicating its good biological safety.

Mechanism underlying the benefits of AuCeNPs is related to the extracellular calcium-sensing receptor

The molecular mechanisms underlying the benefits of AuCeNPs were investigated in isolated PASMCs from rats included in the therapeutic experimental procedure. Specifically, we measured $[Ca^{2+}]_i$ level and evaluated the activity and expression level of the extracellular calcium-sensing receptor (CaSR), an important mediator of pulmonary hypertension as revealed in recent studies including from our lab [5, 6, 40, 42–44]. We found that hypoxia caused a significant increase of $[Ca^{2+}]_i$ (fura 2-ratio=5.29±0.37 versus 3.02±0.35, Fig. 7A and **D**), CaSR activity (fura 2-ratio=10.64±0.67 versus 2.93±0.31, Fig. 7A and **D**) and CaSR expression (1.95-fold versus normoxia, Fig. 7E and **F**) in PASMCs. Moreover, while unmodified CaNPs did not show any benefits (Fig. 7B and **D**), the administration of AuCeNPs reversed hypoxia-induced increase of $[Ca^{2+}]_i$ (3.83±0.29 versus 5.29±0.37, Fig. 7A, C and **D**), CaSR activity (5.72±0.33 versus 10.64±0.67, Fig. 7A, C and **D**) and CaSR expression (1.05-fold versus 1.95-fold for hypoxia, Fig. 7E and **F**). Both CeNPs and AuCeNPs did not affect any of these parameters under normoxia (Fig. 7A-D).

Discussion

Our previous studies have shown that hypoxia induces pulmonary hypertension by an increase in mitochondria-derived reactive oxygen species [6]. In this study, we used AuCeNPs to scavenge excessive ROS production under hypoxic conditions, a phenomenon that comes

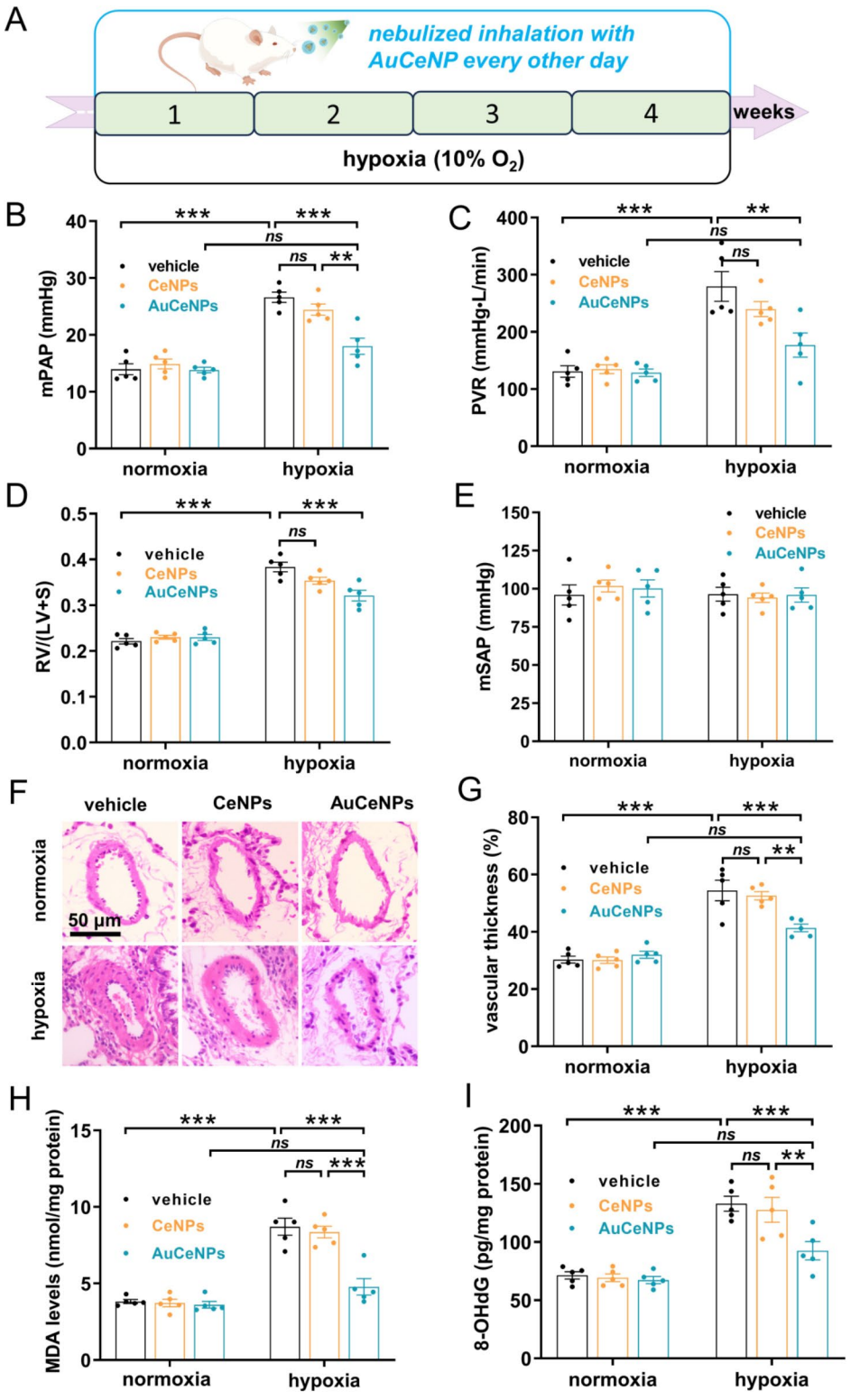

Fig. 5 AuCeNPs prevents hypoxia-induced pulmonary hypertension. The experimental schematic to evaluate the effect of AuCeNPs on hypoxic pulmonary hypertension in preventive mode (**A**). Changes in parameters including mean pulmonary artery pressure (mPAP, **B**), pulmonary vascular resistance (PVR, **C**), right ventricle hypertrophy (RV/[LV + S], **D**), mean systemic arterial pressure (mSAP, **E**), representative HE staining (**F**) and pulmonary vascular wall thickness (pulmonary arteries with diameter 50–100 μm, **G**) in rats, and malondialdehyde (MDA, **H**), 8-hydroxydeoxyguanosine (8-OHdG, **I**) in pulmonary arteries of rats treated with vehicle, CeNPs or AuCeNPs under normoxic or hypoxic conditions. n = 5 rats in each group, $^{***}p < 0.001$, $^{**}p < 0.01$, one-way ANOVA followed by Student-Newman Keuls. LV + S indicates left ventricle plus septum

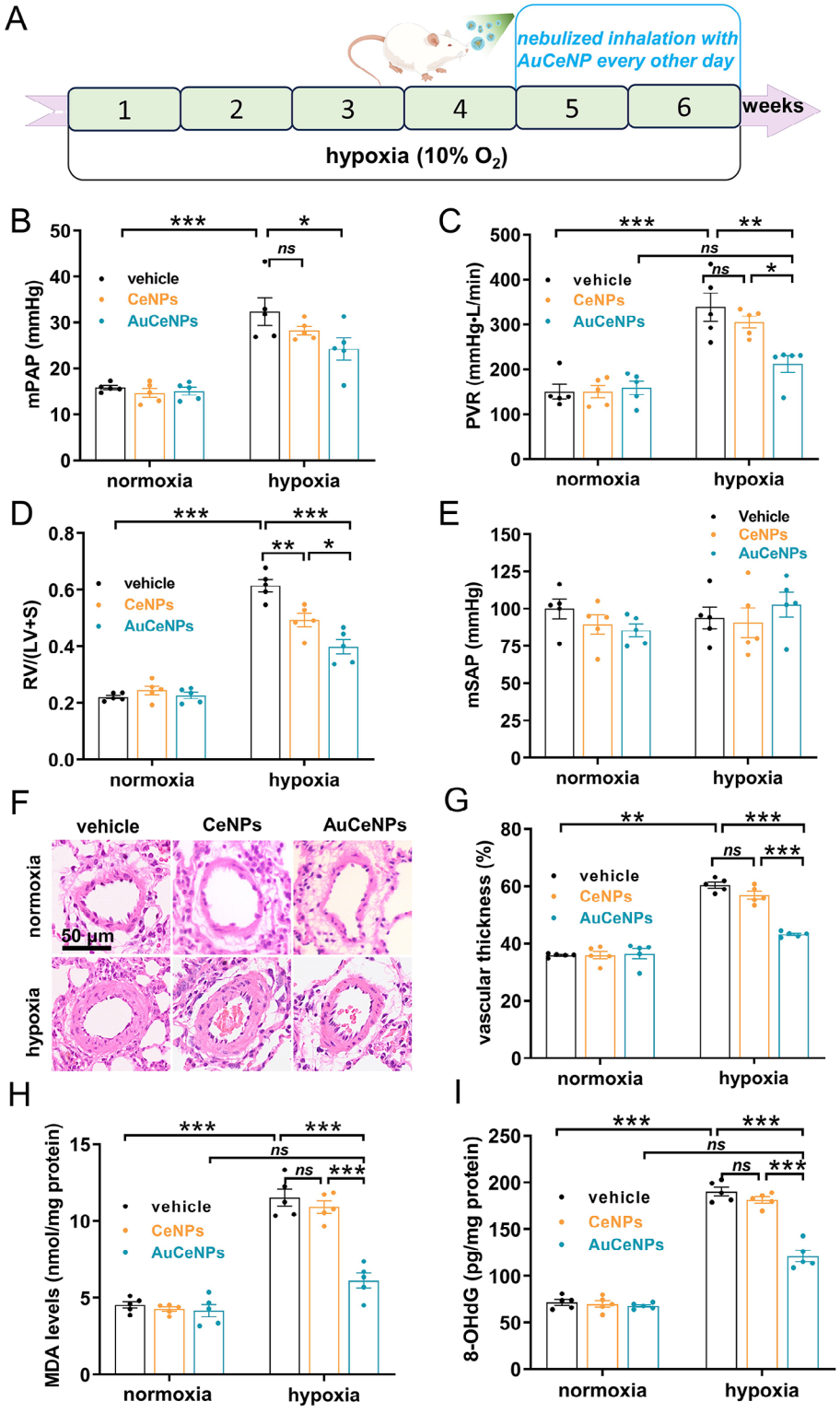

Fig. 6 AuCeNPs reverses hypoxia-induced pulmonary hypertension. The experimental schematic to evaluate the effect of AuCeNPs on hypoxic pulmonary hypertension in therapeutic mode (**A**). Changes in parameters including mean pulmonary artery pressure (mPAP, **B**), pulmonary vascular resistance (PVR, **C**), right ventricle hypertrophy (RV/[LV + S], **D**), mean systemic arterial pressure (mSAP, **E**), representative HE staining (**F**) and pulmonary vascular wall thickness (pulmonary arteries with diameter 50–100 μm, **G**) in rats, and malondialdehyde (MDA, **H**), 8-hydroxydeoxyguanosine (8-OHdG, **I**) in pulmonary arteries of rats treated with vehicle, CeNPs or AuCeNPs under normoxic or hypoxic conditions. n = 5 rats in each group, ***$p < 0.001$, **$p < 0.01$, *$p < 0.05$, one-way ANOVA followed by Student-Newman Keuls. LV + S indicates left ventricle plus septum

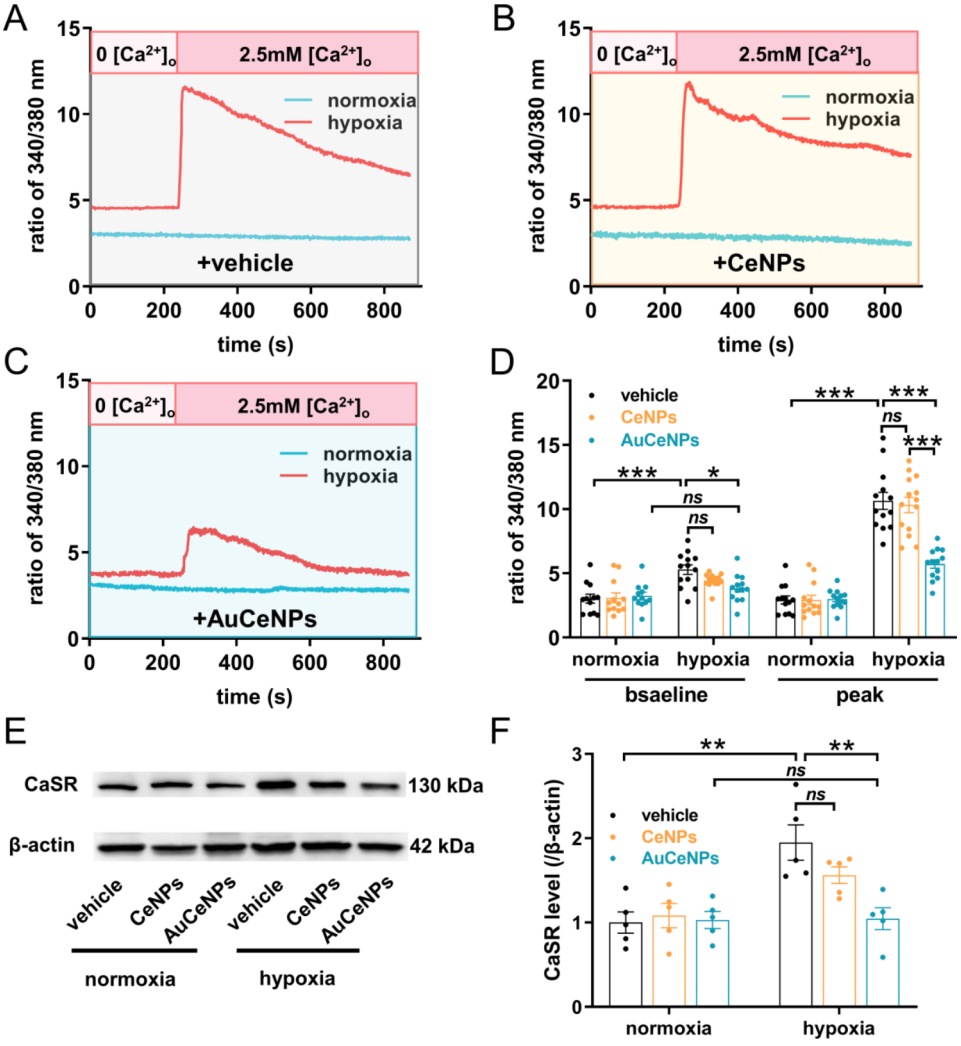

Fig. 7 Mechanisms underlying the benefits of AuCeNPs related to the extracellular calcium-sensing receptor. The representative trace and summarized responses of $[Ca^{2+}]_i$ in pulmonary artery smooth muscle cells (PASMCs) isolated from therapeutic model rats (**A-D**), the representative Western Blot and densitometric levels of extracellular calcium-sensing receptor (CaSR) in PASMCs isolated from therapeutic model rats (**E-F**). ***$p < 0.001$, **$p < 0.01$, *$p < 0.05$, $[Ca^{2+}]_i$ of 12–14 PASMCs from 3 independent rats for each group, one-way ANOVA followed by Student-Newman-Keuls

with a reduction of (i) CaSR activation, (ii) $[Ca^{2+}]_i$, (iii) the proliferation of PASMCs and (iv) hypoxic pulmonary vasoconstriction, ultimately preventing and treating hypoxia-induced pulmonary hypertension.

Due to the large number of reaction sites, CeNPs have persistent antioxidant activity. This is the main difference between classic antioxidants and CeNPs. While usual antioxidants are rapidly oxidized or metabolized, CeNPs maintain their antioxidant effects [45]. In this study, we synthesized a nanozyme (AuCeNPs) with a greater enzymatic activity than commercial unmodified CeNPs by wrapping Au nanoparticles in the center of CeNPs. As shown in Fig. 1, the efficiency of CeNPs in scavenging reactive oxygen species is, however, limited even at high concentration, its efficacy at 200 μg/mL is much lower than AuCeNPs at 40 μg/mL. In terms of CAT or SOD activities, the catalytic activity of AuCeNP at 40 μg/mL is 3.1 and 2.1 times higher, respectively, than CeNP used at a higher dose of 200 μg/mL. The EC50 of AuCeNPs is 74.8 μg/mL (CAT) and 146.2 μg/mL (SOD), while EC50 for CeNPs is 43- and 17-times higher (CAT and SOD, respectively).

For nanomaterials, catalytic activity is related to the exposed catalytic active sites. When the size of nanoparticles decreases and the specific surface area increases, the exposed catalytic active sites will be expected to increase [46, 47]. The size of nanomaterials has also an impact on their absorption. When the size of nanoparticles is small, they can be more easily uptake [48].

In this study, the TEM size of CeNPs was 89 nm, while the TEM size of AuCeNPs was around 30 nm. The specific surface area of AuCeNPs was larger than that of CeNPs, and AuCeNPs are smaller in size. The size of nanoparticles can affect their uptake. The smaller the size

of the nanoparticles, however, does not guarantee the better their absorption. Win et al. investigated the uptake of nanoparticles with different diameters in Caco-2 cells and found that nanoparticles with a size of 100 nm were the most uptake, while nanoparticles with a size higher or lower than 100 nm were lower in uptake than those with a size of 100 nm [49]. Lu et al. reported that silica nanoparticles with a size of 50 nm were the most uptake by cells and the amount of cellular uptake of nanoparticles with a size greater than or less than 50 nm is lower than that of nanoparticles with a size of 50 nm [50]. Chithrani et al. reported that among the three types of cells STO, HELA, and SNB19, Gold Nanoparticles with a diameter of 50 nm had the highest uptake, while Gold Nanoparticles with sizes below 50 nm and above 50 nm had lower uptake than Gold Nanoparticles with sizes of 50 nm [51]. Ding et al. reported that among the three types of cells, 7721, GES-1, and 4T1, Gold nanoparticles with a diameter of 80 nm had the highest uptake, while Gold nanoparticles with a size less than 80 nm had lower uptake than Gold nanoparticles with a size of 80 nm[52]. It seems that an optimal size actually facilitates the better uptake of nanoparticles.

Regarding the influence of shape on the uptake of nanoparticles, Ding et al. reported that there was no significant difference in the absorption of spherical nanomaterials and nanostar (irregular shape) nanoparticles with the same diameter in the three types of cells (7721, GES-1, and 4T1) [52]. Manzanares et al. reported that there is currently no general agreement on whether the nanoparticles shape (sphere-like, cylinders, ellipses, rods, or disks) affects their uptake [53].

To investigate whether there is a difference in the uptake of CeNPs and AuCeNPs in lung tissue and pulmonary artery in the current study, we measured the Ce element content in lung tissue and pulmonary artery of rats receiving CeNPs and AuCeNPs (nebulized inhalation) using ICP-MS. Our supplementary experiments found no difference in Ce uptake by the lung tissue and pulmonary arteries of rats receiving CeNPs and AuCeNPs (Fig. S9).

The main reason for the enhanced catalytic activity of AuCeNPs is the increase in Ce^{3+}/Ce^{4+} and the acceleration of electron transfer by the introduction of Au. The reason is that in our previous study [35], we synthesized two CeNPs (3–4 nm) with sizes much smaller than AuCeNPs (~ 30 nm), which have a larger specific surface area than AuCeNPs, but their catalytic activity is still lower than that of AuCeNPs [35] as also shown Figure S10. So the size difference between CeNPs and AuCeNPs is not the main factor affecting their catalytic activity. The strong catalytic activity exhibited by AuCeNPs avoids simply increasing the dosage to enhance antioxidant activity, as they will aggregate and exhibit toxicity as the dosage increases, ensuring the safety of the application.

The biological safety of CeNPs in rodents through different administration routes has been previously evaluated and the toxicity was dose-dependent [45, 54, 55].

Ma et al. reported that exposure of rats to CeO_2 (at the doses of 0.15, 0.5, 1, 3.5, and 7 mg/kg) caused lung inflammation and toxicity [54]. Another study by Ma et al. reported that a single intratracheal infusion of CeO_2 in rats, at a dose of 3.5 mg/kg, induced the production of fibrosis mediators [55].

In our in vivo study, AuCeNPs were nebulized at a dose of 0.5 mg/kg for four weeks in the prevention protocol or two weeks in the treatment protocol and we did not observe any side effects on plasma Ca^{2+} level, safety blood parameters and liver and renal functions (Figs. S4-S7).

In Ma et al.'s study, CeNPs were reported to be toxic even at low doses, possibly consequently to the aggregation of CeNPs administered through airway infusion [54, 55]. CeNPs have been reported to promote oxidation rather than anti-oxidation in the aggregated state [56–58], which means that once CeNPs aggregate, they will exert a toxic effect. In addition, CeNPs aggregation increases exponentially with increasing concentration [45]. The strong catalytic activity exhibited by AuCeNPs avoids simply increasing the dosage to enhance antioxidant activity, as they will aggregate and exhibit toxicity as the dosage increases, ensuring the safety of the application. We administered AuCeNPs through nebulized inhalation to ensure their uniform and targeted reach to the lungs in a non-aggregated form, so as to prompt them to exert antioxidant effects instead of toxic effects. In addition, the efficiency of nebulized drug delivery to the lungs is about 10% [59–61]. Therefore, considering the dilution factor, the remaining concentration is approximately 0.05 mg/kg, which is a very safe dose [45].

While the ROS scavenging effect of AuCeNPs in pulmonary artery smooth muscle cells (PASMCs) under hypoxia is highly efficient, the nanoparticles did not exert any effect on ROS content in pulmonary artery smooth muscle cells under normoxia. This may be due to the low ROS concentration found in cells under normoxia and a limited activity at low doses of reactants (reaction species).

Although we examined both the preventive and therapeutic potential of AuCeNPs in pulmonary hypertension induced by chronic hypoxia in rats (reproducing group 3 pulmonary hypertension), we haven't examined its benefits in other types of pulmonary hypertension such as pulmonary arterial hypertension (group 1 pulmonary hypertension), pulmonary hypertension due to left heart disease (group 2 pulmonary hypertension) and chronic thromboembolic pulmonary hypertension (group 4

pulmonary hypertension). Additionally, we haven't determined the optimal dosage and the possible long-term side effects on other organs and tissues. All these limitations warrant additional studies in the future as well as the inclusion of both sexes to evaluate potential sex-dependent differences of such therapeutic strategy.

In conclusion, AuCeNPs can not only prevent but also effectively treat hypoxia-induced pulmonary hypertension. The potential underlying mechanism invloves reduction of enhanced CaSR activity and expression in pulmonary artery smooth muscle cells following ROS scavenging. This nanoenzyme provides a new translational preventive and treatment approach for pathologies associated with hypoxic pulmonary hypertension.

Conclusions

Currently, there is no medication available for the treatment of group 3 pulmonary hypertension which is associated with chronic lung disease and/or hypoxia. The modification of ceria nanozyme or nanoparticle (CeNPs) with Au (AuCeNPs) greatly increased its activity for scavenging reactive oxygen species. A small dose of AuCeNPs significantly attenuated hypoxia-induced pulmonary hypertension without showing any obvious side effect(s). AuCeNPs may provide a safe and reliable translational approach for the treatment of group 3 pulmonary hypertension.

Abbreviations

CeNPs	Cerium oxide nanozyme or nanoparticles
AuCeNPs	Wrapping Au in the center of cerium oxide nanoparticles
CaSR	Extracellular calcium-sensing receptor
ROS	Reactive oxygen species
PASMCs	Pulmonary artery smooth muscle cells
$[Ca^{2+}]_i$	Intracellular Ca^{2+} concentration
SOD	Superoxide dismutase
CAT	Catalase
MCT	Monocrotaline
NBT	Nitrotetrazolium blue chloride
MTT	Methylthiazolyldiphenyl-tetrazolium bromide
HUVEC	Human umbilical vein endothelial thin
TEM	Transmission electron microscopy
HRTEM	High-resolution transition electron microscopy
XPS	X-ray photoelectron spectroscopy
mPAP	Mean pulmonary artery pressure
PVR	Pulmonary vascular resistance
RV	Right ventricle free wall
LV + S	Left ventricle with interventricular septum

Supplementary Information

The online version contains supplementary material available at https://doi.org/10.1186/s12951-024-02738-4.

Supplementary Material 1

Acknowledgements

We sincerely appreciate the Experimental Animal Center of Huazhong University of Science and Technology for its full support of this study.

Author contributions

QH and ZW established the study conception; QH, ZW, LW, LZ, RX, Jia Liu and LS devised the experiments; QH, ZW, LW, LZ, RX, Jia Liu, LS, TZ, Jie Liu, SQ, MR and JD executed the data analyses and interpretation; RX, Jia Liu, LS, TZ, Jie Liu, and QS performed the data acquisition; QH, RX, Jia Liu, ZW, LW, LZ, LS, MR and JD prepared the article. All authors approved the final version of article.

Funding

This study was supported by grants from the National Natural Science Foundation of China (grant numbers 82241014, 82130002, 82170068 and 82270060) and Natural Science Foundation of Hubei Province (2024AFA053).

Data availability

No datasets were generated or analysed during the current study.

Declarations

Ethics approval and consent to participate

All procedures performed in animals were approved by the Institutional Animal Care and Use Committee of Tongji Medical College, Huazhong University of Science and Technology, and according to the guidance of the National Institutes of Health.

Consent for publication

All authors are aware of and agree to the content of the paper and their being listed as a co-author of the paper.

Competing interests

The authors declare no competing interests.

Author details

[1]Department of Pathophysiology, School of Basic Medicine, Tongji Medical College, Huazhong University of Science and Technology (HUST), 13 Hangkong Road, Wuhan 430030, China
[2]Key Laboratory of Pulmonary Diseases of Ministry of Health, Tongji Medical College, HUST, Wuhan, China
[3]Research Center for Tissue Engineering and Regenerative Medicine, Union Hospital, Tongji Medical College, HUST, Wuhan, China
[4]Department of Clinical Laboratory, Union Hospital, Tongji Medical College, HUST, Wuhan, China
[5]Department of Nutrition, Université de Montréal, Montreal, Canada
[6]Montreal Heart Institute, Montréal, Québec, Canada
[7]Department of medicine, Université de Montréal, Montréal, Québec, Canada
[8]Department of Gastrointestinal Surgery, Union Hospital, Tongji Medical College, HUST, Wuhan, China

Received: 23 November 2023 / Accepted: 24 July 2024
Published online: 19 August 2024

References

1. Humbert M, Morrell NW, Archer SL, Stenmark KR, MacLean MR, Lang IM, et al. Cellular and molecular pathobiology of pulmonary arterial hypertension. J Am Coll Cardiol. 2004;43:S13–24.
2. Culley MK, Chan SY. Endothelial senescence: a new age in pulmonary hypertension. Circ Res. 2022;130:928–41.
3. Boucherat O, Agrawal V, Lawrie A, Bonnet S. The latest in animal models of pulmonary hypertension and right ventricular failure. Circ Res. 2022;130:1466–86.
4. Humbert M, Kovacs G, Hoeper MM, Badagliacca R, Berger RMF, Brida M, ESC/ERS Scientific Document Group, et al. 2022 ESC/ERS guidelines for the diagnosis and treatment of pulmonary hypertension. Eur Heart J. 2022;43:3618–731.
5. Zhang J, Zhou J, Cai L, Lu Y, Wang T, Zhu L, et al. Extracellular calcium-sensing receptor is critical in hypoxic pulmonary vasoconstriction. Antioxid Redox Signal. 2012;17:471–84.
6. Xiao R, Luo S, Zhang T, Lv Y, Wang T, Zhang J, et al. Peptide blocking self-polymerization of extracellular calcium-sensing receptor attenuates hypoxia-induced pulmonary hypertension. Hypertension. 2021;78:1605–16.

7. Waypa GB, Marks JD, Guzy R, Mungai PT, Schriewer J, Dokic D, et al. Hypoxia triggers subcellular compartmental redox signaling in vascular smooth muscle cells. Circ Res. 2010;106:526–35.
8. Desireddi JR, Farrow KN, Marks JD, Waypa GB, Schumacker PT. Hypoxia increases ROS signaling and cytosolic Ca^{2+} in pulmonary artery smooth muscle cells of mouse lungs slices. Antioxid Redox Signal. 2010;12:595–602.
9. Pak O, Scheibe S, Esfandiary A, Gierhardt M, Sydykov A, Logan A et al. Impact of the mitochondria-targeted antioxidant MitoQ on hypoxia-induced pulmonary hypertension. Eur Respir J. 2018:1701024.
10. Ahmed MN, Zhang Y, Codipilly C, Zaghloul N, Patel D, Wolin M, et al. Extracellular superoxide dismutase overexpression can reverse the course of hypoxia-induced pulmonary hypertension. Mol Med. 2012;18:38–46.
11. Adesina SE, Kang BY, Bijli KM, Ma J, Cheng J, Murphy TC, et al. Targeting mitochondrial reactive oxygen species to modulate hypoxia-induced pulmonary hypertension. Free Radic Biol Med. 2015;87:36–47.
12. Kang Y, Zhang G, Huang EC, Huang J, Cai J, Cai L, et al. Sulforaphane prevents right ventricular injury and reduces pulmonary vascular remodeling in pulmonary arterial hypertension. Am J Physiol Heart Circ Physiol. 2020;318:H853–66.
13. Budas GR, Boehm M, Kojonazarov B, Viswanathan G, Tian X, Veeroju S, et al. ASK1 inhibition halts disease progression in preclinical models of pulmonary arterial hypertension. Am J Respir Crit Care Med. 2018;197:373–85.
14. Zhang R, Fan K, Yan X. Nanozymes: created by learning from nature. Sci China Life Sci. 2020;63:1183–200.
15. Wu J, Wang X, Wang Q, Lou Z, Li S, Zhu Y, et al. Nanomaterials with enzyme-like characteristics (nanozymes): next-generation artificial enzymes (II). Chem Soc Rev. 2019;48:1004–76.
16. Ai Y, Hu Z, Liang X, Sun H, Xin H, Liang Q. Recent advances in nanozymes: from matters to bioapplications. Adv Funct Mater. 2021;32:2110432.
17. Zhang C, Wang X, Du J, Gu Z, Zhao Y. Reactive oxygen species-regulating strategies based on nanomaterials for disease treatment. Adv Sci. 2021;8:2002797.
18. Chung D. Nanoparticles have health benefits too. New Sci. 2003;179:2410–6.
19. Tarnuzzer RW, Colon J, Patil S, Seal S. Vacancy engineered ceria nanostructures for protection from radiation-induced cellular damage. Nano Lett. 2005;5:2573–7.
20. Niu J, Azfer A, Rogers LM, Wang X, Kolattukudy PE. Cardioprotective effects of cerium oxide nanoparticles in a transgenic murine model of cardiomyopathy. Cardiovasc Res. 2007;73:549–59.
21. Das S, Dowding JM, Klump KE, McGinnis JF, Self W, Seal S. Cerium oxide nanoparticles: applications and prospects in nanomedicine. Nanomed (Lond). 2013;8:1483–508.
22. Arya A, Sethy NK, Singh SK, Das M, Bhargava K. Cerium oxide nanoparticles protect rodent lungs from hypobaric hypoxia-induced oxidative stress and inflammation. Int J Nanomed. 2013;8:4507–20.
23. Gubernatorova EO, Liu X, Othman A, Muraoka WT, Koroleva EP, Andreescu S et al. Europium-doped cerium oxide nanoparticles limit reactive oxygen species formation and ameliorate intestinal ischemia-reperfusion injury. Adv Healthc Mater. 2017;6.
24. Ni D, Wei H, Chen W, Bao Q, Rosenkrans ZT, Barnhart TE, et al. Ceria nanoparticles meet hepatic ischemia-reperfusion injury: the perfect imperfection. Adv Mater. 2019;31:e1902956.
25. Li X, Han Z, Wang T, Ma C, Li H, Lei H, et al. Cerium oxide nanoparticles with antioxidative neurorestoration for ischemic stroke. Biomaterials. 2022;291:121904.
26. Dong S, Dong Y, Jia T, Liu S, Liu J, Yang D, He F, Gai S, Yang P, Lin J. GSH-depleted nanozymes with hyperthermia-enhanced dual enzyme-mimic activities for tumor nanocatalytic therapy. Adv Mater. 2020;32:e2002439.
27. Liu J, Liu C, Tang J, Chen Q, Yu Y, Dong Y, Hao J, Wu W. Synergistic cerium oxide nanozymes: targeting DNA damage and alleviating tumor hypoxia for improved NSCLC radiotherapy efficiency. J Nanobiotechnol. 2024;22:25.
28. Kwon HJ, Kim D, Seo K, Kim YG, Han SI, Kang T, et al. Ceria nanoparticle systems for selective scavenging of mitochondrial, intracellular, and extracellular reactive oxygen species in Parkinson's disease. Angew Chem Int Ed Engl. 2018;57:9408–12.
29. Li M, Shi P, Xu C, Ren J, Qu X. Cerium oxide caged metal chelator: anti-aggregation and anti-oxidation integrated H_2O_2-responsive controlled drug release for potential Alzheimer's disease treatment. Chem Sci. 2013;4:2536–42.
30. Amin KA, Hassan MS, Awad el-ST, Hashem KS. The protective effects of cerium oxide nanoparticles against hepatic oxidative damage induced by monocrotaline. Int J Nanomed. 2011;6:143–9.
31. Kolli MB, Manne NDPK, Para R, Nalabotu SK, Nandyala G, Shokuhfar T, et al. Cerium oxide nanoparticles attenuate monocrotaline induced right ventricular hypertrophy following pulmonary arterial hypertension. Biomaterials. 2014;35:9951–62.
32. Nassar SZ, Hassaan PS, Abdelmonsif DA, ElAchy SN. Cardioprotective effect of cerium oxide nanoparticles in monocrotaline rat model of pulmonary hypertension: a possible implication of endothelin-1. Life Sci. 2018;201:89–101.
33. Heckert EG, Karakoti AS, Seal S, Self WT. The role of cerium redox state in the SOD mimetic activity of nanoceria. Biomaterials. 2008;29:2705–9.
34. Celardo I, Pedersen JZ, Traversa E, Ghibelli L. Pharmacological potential of cerium oxide nanoparticles. Nanoscale. 2011;3:1411–20.
35. Li M, Liu J, Shi L, Zhou C, Zou M, Fu D, et al. Gold nanoparticles-embedded ceria with enhanced antioxidant activities for treating inflammatory bowel disease. Bioact Mater. 2023;25:95–106.
36. Jian B, Yang S, Chen D, Zou L, Chatham JC, Chaudry I, et al. Aging influences cardiac mitochondrial gene expression and cardiovascular function following hemorrhage injury. Mol Med. 2011;17:542–9.
37. Lyon AR, Joudrey PJ, Jin D, Nass RD, Aon MA, O'Rourke B, et al. Optical imaging of mitochondrial function uncovers actively propagating waves of mitochondrial membrane potential collapse across intact heart. J Mol Cell Cardiol. 2010;49:565–75.
38. Li J, Song S, Long Y, Wu L, Wang X, Xing Y et al. Investigating the hybrid-structure-effect of CeO_2-encapsulated au nanostructures on the transfer coupling of nitrobenzene. Adv Mater. 2018;30.
39. Miao Z, Jiang S, Ding M, Sun S, Ma Y, Younis MR, et al. Ultrasmall rhodium nanozyme with RONS scavenging and photothermal activities for anti-inflammation and antitumor theranostics of colon diseases. Nano Lett. 2020;20:3079–89.
40. Zeng X, Zhu L, Xiao R, Liu B, Sun M, Liu F, et al. Hypoxia-induced mitogenic factor acts as a nonclassical ligand of calcium-sensing receptor, therapeutically exploitable for intermittent hypoxia-induced pulmonary hypertension. Hypertension. 2017;69:844–54.
41. Ziegelstein RC, Xiong Y, He C, Hu Q. Expression of a functional extracellular calcium-sensing receptor in human aortic endothelial cells. Biochem Biophys Res Commun. 2006;342:153–63.
42. Zhu L, Liu F, Hao Q, Feng T, Chen Z, Luo S, et al. Dietary geranylgeranyl pyrophosphate counteracts the benefits of statin therapy in experimental pulmonary hypertension. Circulation. 2021;143:1775–92.
43. Xiao R, Liu J, Luo S, Yu Z, Zhang J, Lv Y, et al. Orally-administrated mitochondria attenuate pulmonary hypertension with the aid of erythrocytes as carriers. Clin Transl Med. 2022;12:e1033.
44. Yamamura A, Guo Q, Yamamura H, Zimnicka AM, Pohl NM, Smith KA, et al. Enhanced Ca^{2+}-sensing receptor function in idiopathic pulmonary arterial hypertension. Circ Res. 2012;111:469–81.
45. Casals E, Zeng M, Parra-Robert M, Fernández-Varo G, Morales-Ruiz M, Jiménez W, et al. Cerium oxide nanoparticles: advances in biodistribution, toxicity, and preclinical exploration. Small. 2020;16:e1907322.
46. Yuan MJ, Li Q, Gao Y, He C, Adli M, Wu CZ, et al. Tunable structured metal oxides for biocatalytic therapeutics. Adv Funct Mater. 2023;33(40):2304271.
47. Sheng J, Wu Y, Ding H, Feng K, Shen Y, Zhang Y, et al. Multienzyme-like nanozymes: regulation, rational design, and application. Adv Mater. 2024;36:e2211210.
48. Buzea C, Pacheco II, Robbie K. Nanomaterials and nanoparticles: sources and toxicity. Biointerphases. 2007;2:MR17–71.
49. Win KY, Feng SS. Effects of particle size and surface coating on cellular uptake of polymeric nanoparticles for oral delivery of anticancer drugs. Biomaterials. 2005;26:2713–22.
50. Lu F, Wu SH, Hung Y, Mou CY. Size effect on cell uptake in well-suspended, uniform mesoporous silica nanoparticles. Small. 2009;5:1408–13.
51. Chithrani BD, Chan WC. Elucidating the mechanism of cellular uptake and removal of protein-coated gold nanoparticles of different sizes and shapes. Nano Lett. 2007;7:1542–50.
52. Ding L, Yao C, Yin X, Li C, Huang Y, Wu M, et al. Size, shape, and protein corona determine cellular uptake and removal mechanisms of gold nanoparticles. Small. 2018;14:e1801451.
53. Manzanares D, Ceña V, Endocytosis. The nanoparticle and submicron nanocompounds gateway into the cell. Pharmaceutics. 2020;12:371.
54. Ma JY, Zhao H, Mercer RR, Barger M, Rao M, Meighan T, et al. Cerium oxide nanoparticle-induced pulmonary inflammation and alveolar macrophage functional change in rats. Nanotoxicology. 2011;5:312–25.
55. Ma J, Bishoff B, Mercer RR, Barger M, Schwegler-Berry D, Castranova V. Role of epithelial-mesenchymal transition (EMT) and fibroblast function in

cerium oxide nanoparticles-induced lung fibrosis. Toxicol Appl Pharmacol. 2017;323:16–25.
56. Dowding JM, Das S, Kumar A, Dosani T, McCormack R, Gupta A, et al. Cellular interaction and toxicity depend on physicochemical properties and surface modification of redox-active nanomaterials. ACS Nano. 2013;7:4855–68.
57. Rogers S, Rice KM, Manne ND, Shokuhfar T, He K, Selvaraj V, et al. Cerium oxide nanoparticle aggregates affect stress response and function in Caenorhabditis elegans. SAGE Open Med. 2015;3:2050312115575387.
58. Feliu N, Docter D, Heine M, Del Pino P, Ashraf S, Kolosnjaj-Tabi J, et al. In vivo degeneration and the fate of inorganic nanoparticles. Chem Soc Rev. 2016;45:2440–57.
59. Newman SP. Aerosol deposition considerations in inhalation therapy. Chest. 1985;88:S152–60.
60. Johnson MA, Newman SP, Bloom R, Talaee N, Clarke SW. Delivery of albuterol and ipratropium bromide from two nebulizer systems in chronic stable asthma. Efficacy and pulmonary deposition. Chest. 1989;96:6–10.
61. Mashat M, Clark BJ, Assi KH, Chrystyn H. In vitro aerodynamic characterization of the dose emitted during nebulization of tobramycin high strength solution by novel and jet nebulizer delivery systems. Pulm Pharmacol Ther. 2016;37:37–42.

Publisher's Note